Dalton Transactions

Accepted Manuscript

ROYAL SOCIETY OF CHEMISTRY

www.rsc.org/dalton

Journal Name

RSCPublishing

ARTICLE

Pathogenic Properties of Alzheimer's β-Amyloid Identified from Structure-Property Patient-Phenotype Correlations

Manish K. Tiwari and Kasper P. Kepp*

Cite this: DOI: 10.1039/x0xx00000x

Received 00th January 2012,
Accepted 00th January 2012

DOI: 10.1039/x0xx00000x

www.rsc.org/

β-amyloid (Aβ) plays a central role in Alzheimer's disease (AD), but the specific molecular mechanism and associated structures remain unknown. We compiled patient data for carriers of genetic variants of Aβ that cause AD and correlated these data against chemical properties for 56 mutant conformations derived from four published experimental conformations of Aβ of variable structure and chemical environment. Disease onset of variants is significantly ($p \sim 0.006$) correlated to hydrophobic surfaces of disordered conformations (2LFM), whereas structured conformations yielded no correlations. Correlation also applied ($p < 0.03$) to *in vitro* steady-state Aβ levels. We conclude that disordered monomers are likely to be pathogenically important in contrast to structured conformations and that hydrophobic surface correlates with pathogenesis. This first established correlation between clinical and chemical data suggests that specific exposed, disordered monomers are viable targets for AD therapy.

Introduction

The major neurodegenerative disease Alzheimer's disease (AD) is characterized by impaired memory, gradual decline of cognitive abilities, and personality changes.[1-5] It mostly occurs sporadically with no apparent inheritance,[6] a broad clinical spectrum,[3] and with age as the largest among many risk factors of small, but cumulative significance.[1, 7] Genetically inherited AD accounts for ~5% of all cases and cause particularly severe, early-onset familial AD (FAD), most notably due to mutations in the enigmatic, transmembrane Amyloid Precursor Protein (APP) or in presenilin (PSEN), which forms part of the γ-secretase complex that degrades APP.[8, 9]

The central hallmark of AD is extracellular deposits of senile plaques consisting of β-amyloid (Aβ) peptides, which are proteolytic cleavage products of APP found in the membranes of cells and organelles.[1, 10] For this reason and because of the FAD genetic risk factors relating to APP or its processing, Aβ is thought to play a central role in AD viz. the "Amyloid Cascade Hypothesis", i.e. that overload of Aβ causes disease.[11]

However, neurodegeneration and cognitive decline are not generally correlated with plaque Aβ levels,[12] and some genetic risk factors such as PSEN1 variants actually reduce total Aβ levels.[13] Consequently, focus has changed towards longer Aβ isoforms such as $A\beta_{42}$ and in particular the ratio between long and short isoforms (notably $A\beta_{42}/A\beta_{40}$) and small soluble oligomers of Aβ as the perceived toxic species[14, 15] that damage neuronal cells[14, 16] and tend to follow disease progression.[17]

Polypeptide misfolding due to exposure of hydrophobic protein parts is considered a major driving force behind processes leading to oligomers and fibrils.[18, 19] Given its role in Alzheimer's Disease, during the last decades, structural and dynamic studies of Aβ species have emerged,[20, 21] including mature Aβ fibrils,[20, 22] protofibrils,[23] oligomers[24] and various polymorphisms.[21, 25] These species generally contain substantial β-sheet character typical of aggregates and fibrillar peptide deposits. Despite the renewed focus on small soluble forms of Aβ, soluble Aβ monomers, which form critical intermediates that are precursors Aβ misfolding,[26-29] have not been comprehensively studied, partly because these monomers, in contrast to aggregates, are disordered in solution with little β-sheet and only some α-helix character.[30]

The neurotoxicity of Aβ is thought to be highly conformation and environment dependent[31] and, as specifically utilized in the present work, conformations and hydrophobic exposure is highly environment-dependent both for fibrils[28, 32, 33] and monomers, as evident in NMR structures.[34, 35] Conformation and size-dependent hydrophobic properties may determine the pathogenicity of small $A\beta_{42}$ oligomers rather the presence of β-sheet aggregates.[36, 37] Previous NMR[38] and computational[39] studies have shown that the hydrophobicity arising from central and C-terminal regions of Aβ is responsible for formation of an extended β-sheet confirmation with a connecting turn between them. This "hairpin" topology is suggested to resemble Aβ in their fibril forms.[40]

Despite this, the conformations, sizes, and specific pathogenic molecular modes of action remain unknown, partly because patient data cannot be correlated directly to these forms *in vivo*.[13, 41] Thus, identifying the causative molecular species and chemical properties of Aβ remains a primary priority.

We report here the analysis of compiled data for patients carrying genetic variants of Aβ known to cause disease, correlated against robust measures of hydrophobic surface areas and other chemical properties derived from four different experimental structures of wild-type Aβ monomers, two for $A\beta_{42}$ and two for $A\beta_{40}$. These four structures mimic variable *in-vivo* environments by representing a spectrum from 100% water (2LFM[42]), via 80% and 70% water (1IYT,[35] 1ZOQ[43]) to a water-micelle like environment representative of membrane-interacting species (1BA4[34]). They also represent a hierarchy from little structure (2LFM and to some extent 1BA4) to more structured (1IYT, 1Z0Q).

Importantly, we establish a correlation between patient age of disease onset (t_{onset}, in years) and hydrophobic exposure in the disordered conformations (in particular 2LFM), but not the more

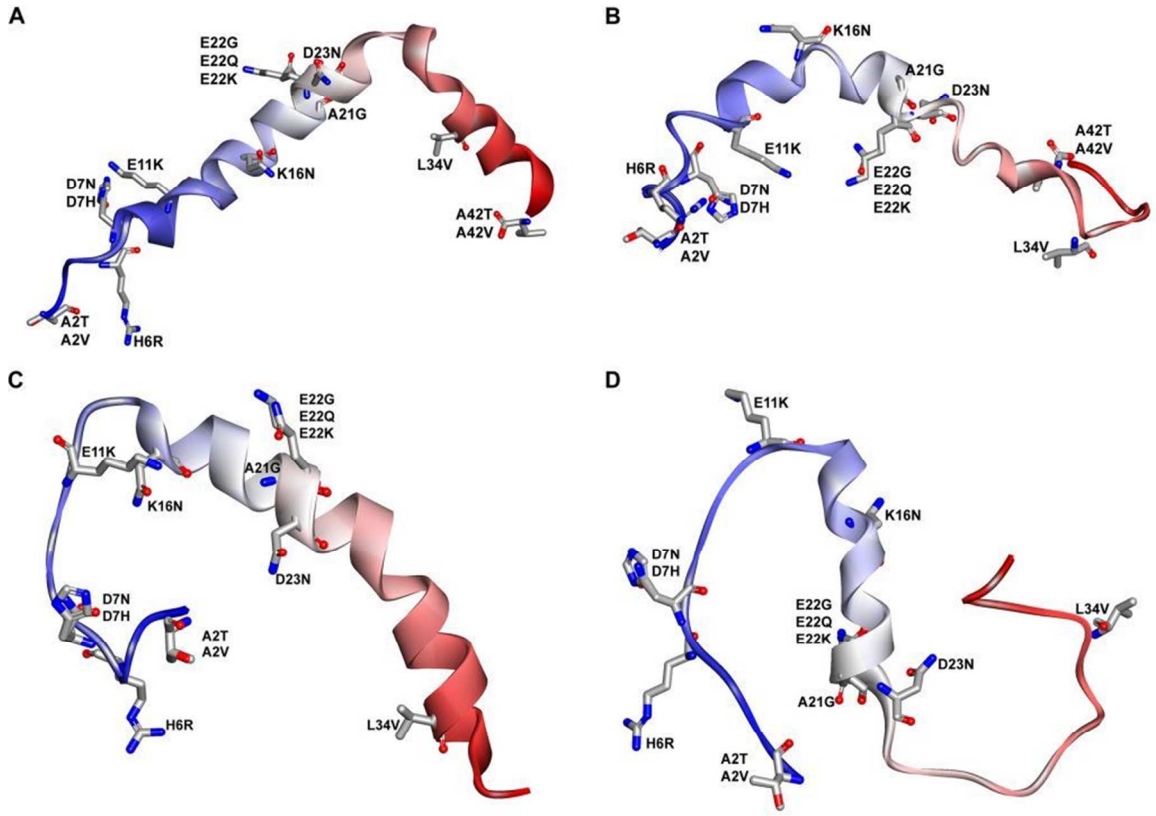

Figure 1. Wild-type and mutant structures of $A\beta_{42}$ and $A\beta_{40}$. (A, B) The NMR structure of wild-type $A\beta_{42}$ (PDB codes 1IYT and 1Z0Q) and their 15 superimposed computational structures of $A\beta_{42}$ mutants. (C, D) The NMR structure of wild-type $A\beta_{40}$ (PDB codes 1BA4 and 2LFM) and their 13 superimposed structures of $A\beta_{40}$ mutants. The mutant residues are shown in stick-model. The peptide's secondary structure is shown with blue N-terminus and red C-terminus (the figure was generated using Discovery Studio (DS) 4.0 visualizer).

structured conformations. This indicates that hydrophobic exposure is a pathogenically relevant property for disordered amyloid species, but not for the more structured amyloids. The statistical significance of this observation is unlikely to be coincidental (confidence level > 99%) and thus implies that structural features resembling the 2LFM conformation are related to disease, e.g. as the relevant precursor properties leading to oligomers in AD. These findings suggest a change of focus towards controlling disordered and exposed monomer species in AD, with the 2LFM structure providing the template for such structure-based design.

Results and discussion

15 known missense mutations and one deletion (E693Δ, corresponding to E22Δ in Aβ numbering) within the $A\beta_{42}$ region of APP are associated with FAD or cerebral amyloid angiopathy (Figure 1A and 1B). $A\beta_{40}$ is represented by only 13 mutations (Figure 1C and 1D) since two variations occur at position 42.

56 mutant structures were derived from the four initial structures of $A\beta_{42}$ (1IYT and 1Z0Q) and $A\beta_{40}$ (1BA4 and 2LFM) (Figures S1, S2, S3 and S4). To preserve the experimental time-averaged conformational properties, the original backbone and non-mutated side-chain conformations were preserved during modeling.[44] Hydrogen atoms were added using the CHARMM force field[45] and protonation states for ionizable residues were manually verified for all 60 (four wild-type and 56 mutant) structures before analysis. The mutant conformations were constructed as described in the Methods section.

From the experimentally derived structures, we computed the total solvent accessible surface area (SAS) and the hydrophobic and hydrophilic surfaces for all wild-type and mutant structures. To account for method dependence, we used four different methods (see computational methods section) to compute SAS for each structure individually (Tables S1, S2, S3, and S4). All methods give very similar results, except for one K16N-1BA4$A\beta_{40}$ mutation (Figure S5), which has minor effect on the overall correlation. To further test result sensitivity, we correlated total SAS from Discovery Studio 4.0 and StrucTools (Figure S7) for each structure. Strong correlations between the two sets of data for the same structure were observed (Figure S7).

We further calculated the hydrophobic and hydrophilic surface areas for all structures (Tables S5, S6, S7 and S8). We tested the structural sensitivity by correlating hydrophilic and hydrophobic surfaces of each pair of structures (1IYT vs. 1Z0Q; $A\beta_{42}$ and 1BA4 vs. 2LFM; $A\beta_{40}$) (Figure S8). These correlations show significant similarities as expected for the same peptides but also clear indications of conformational differences, with $R^2 \sim 0.77-0.96$, $p < 0.001$ (Figures S8A, 8B, 8C, and 8D). From these sensitivity tests, we thus find that the applied methodology produces robust data for analysis.

For the studied genetic variants, we collected all relevant, available data on patient t_{onset} and total Aβ levels observed for a given variant in cell studies (Tables S9 and S10). Patient t_{onset} was not significantly correlated with total SAS or hydrophilic surfaces of $A\beta_{42}$ and $A\beta_{40}$ (Figures S9 and S10; Tables S11, S12, S13, and S14)

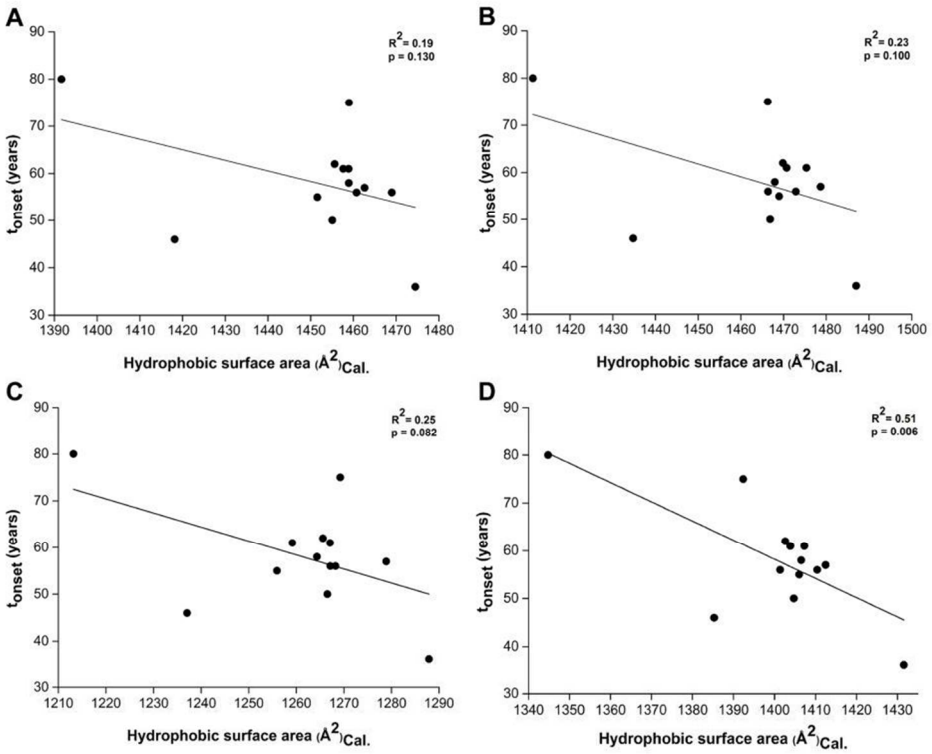

Figure 2. Correlation between t_{onset} and calculated hydrophobic surface for WT and mutant $A\beta_{40}$ and $A\beta_{42}$. (A) vs. 1IYT WT and mutants $A\beta_{42}$. (B) vs. 1Z0Q WT and mutants $A\beta_{42}$. (C) vs. 1BA4 WT and mutants $A\beta_{40}$. (D) vs. 2LFM WT and mutants $A\beta_{40}$.

but was significantly correlated to hydrophobic surface of the disordered structures (Figure 2). Correlation of t_{onset} to hydrophobic surface was strongly conformation-dependent: 1IYT gave $R^2 = 0.19$; $p = 0.13$ (Figure 2A), 1Z0Q gave $R^2 = 0.23$; $p = 0.10$ (Figure 2B), 1BA4 had $R^2 = 0.25$; $p = 0.08$ (Figure 2C), and 2LFM had $R^2 = 0.51$; $p = 0.006$; (Figure 2D). Importantly, the correlation follows a trend of structure: To substantiate this, we calculated the helical percentage for the 60 structures (Table S15). The structure 2LFM that showed strong statistically significant correlation to t_{onset} contains the least helix character (22.5%).

Thus, our analysis shows that among the two major isoforms of amyloid in the brain, only disordered structural features represented by 2LFM have pathogenic properties, and these relate to exposure of hydrophobic surface. Surface compositions of Aβ have previously been suggested to be determinants of Aβ-induced neurotoxicity in AD progression.[46, 47] As seen, hydrophobic exposure can explain real patient data from one specific, disordered conformation of the peptide, providing the first statistically significant link (at the 99% significance level) between clinical and chemical data in this field. The significance suggests that, despite well-known heterogeneities in lab protocols of the original experiments, upon proper normalization of data to their respective wild-type values, the probability that the presently identified correlations are coincidental is smaller than 1%.

Our observed relation between exposed hydrophobic surface and patient disease onset is consistent with previous mutagenesis studies that focused on the C-terminal of both $A\beta_{40}$ and $A\beta_{42}$: These studies found that improved hydrophobic exposure and interaction between putative β-sheets increase the stability of the hairpin structure.[48] The oligomerization of monomers likely occurs by disorder, exposure, and concomitant α-to-β transitions.

Aβ-induced cytotoxicity has been the subject of intense research. Recently Aβ's ability to mediate cytotoxicity via membrane disruption has received particular notice.[49] The mechanism of Aβ interaction with membranes remains to be further elucidated, but recent insight suggests that cell surface interactions are a prerequisite for cytotoxicity.[50, 51] Such a membrane-association mechanism is consistent with the exposed hydrophobic conformations identified as pathogenic in our work.

Finally, we also correlated *in vitro* total steady-state Aβ levels for the variants against chemical properties (Tables S16, S17, S18 and S19). Interestingly, except for the hydrophobic surface (Figure 3), again the studied properties yielded insignificant or no correlation with Aβ levels (Figures S11 and S12). Only the hydrophobic surface area of the least structured (22.5% helix) 2LFM conformation (Figure 3D) was significantly correlated with steady-state levels at the 97% confidence level ($R^2 = 0.36$; $p = 0.03$). This suggests that the same chemical properties that relate to pathogenicity of the monomer (i.e. hydrophobic exposure) also relate to increased steady-state amyloid levels. Thus, hydrophobic exposure in the fully solvated disordered monomer is related to amyloid buildup in genetic variants, whereas other conformations did not relate to amyloid buildup.

Concluding remarks

In conclusion, we have established the first significant link between chemical properties of specific amyloid structures and real Alzheimer patient data at the 99% confidence level ($p \sim 0.006$) and identified particular disordered monomers (the 2LFM conformations) as related to pathogenesis. The correlation of both amyloid steady-state levels and disease onset to the same chemical property of disordered amyloids may explain why amyloid levels

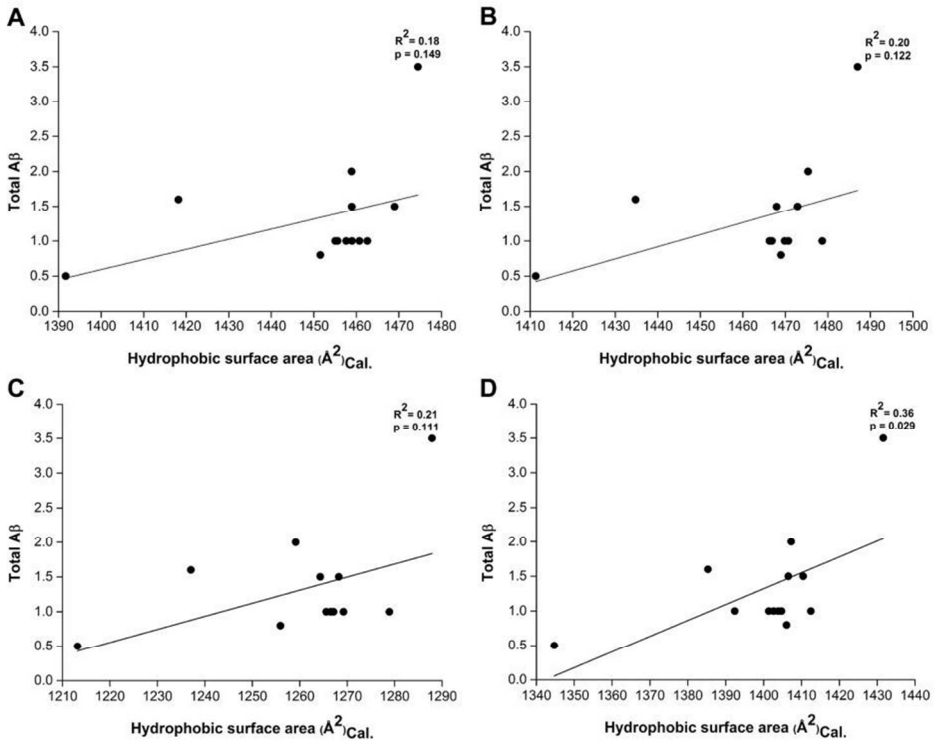

Figure 3. Correlation between total Aβ levels and calculated hydrophobic surface for WT and mutant $A\beta_{40}$ and $A\beta_{42}$. (A) vs. 1IYT WT and mutants $A\beta_{42}$. (B) vs. 1Z0Q WT and mutants $A\beta_{42}$. (C) vs. 1BA4 WT and mutants $A\beta_{40}$. (D) vs. 2LFM WT and mutants $A\beta_{40}$.

have been mistaken for pathogenic in earlier work leading to the classical "cascade" hypotheses. In fact, our analysis suggests that mainly the hydrophobic surface relates to disease.

The identified changes are caused by genetic variation in the Aβ variants studied in this work, but could conceivably be caused by post-translational modifications such as metal binding, phosphorylation, or oxidation, in the major sporadic forms of the disease,[52] providing perspectives for unifying the two forms. It has not escaped our attention that metal binding would immediately reduce the net negative charge from −3 to −1 and increase hydrophobicity of the amyloids, providing a "sporadic" counterpart to the familial AD mechanism described in the present work. Also, the identification of 2LFM-like features as potentially pathogenic provides perspectives for molecular targeting of specific disordered amyloid species in line with recent work in this direction.[53, 54]

The statistically significant correlations obtained in this study suggest that the heterogeneity in various lab protocols is not a major issue; and similar approaches could be utilized to rationalize relationships between structure and clinical phenotype for related disorders, in particular as patient data become more generally available.

Material and methods

Starting Structural Models and properties calculation

Initial coordinates of solution NMR WT structures for $A\beta_{42}$ (PDB: 1IYT[35] and 1ZOQ[43]) and $A\beta_{40}$ (PDB: 1BA4[34] and 2LFM[42]) were extracted from the RCSB Protein Data Bank (www.rcsb.org/pdb/). To mimic the physiological states, protonation states for ionizable residues in both $A\beta_{42}$ and $A\beta_{40}$ peptides were applied as suitable for a physiological pH, with both arginine and lysine residues modeled as positively charged and glutamic and aspartic acids as deprotonated. Histidine residues were modeled as neutral with only the δ nitrogen protonated. The N and C termini were chosen to be protonated and deprotonated, respectively, in both $A\beta_{42}$ and $A\beta_{40}$ peptides and employed as starting structure for mutant modeling.

Mutant modeling

The mutant structures were constructed by *in silico* by mutating the wild-type (WT) structure[44] using the protein design extension in Discovery Studio 4.0 (DS 4.0, Accelrys Inc., San Diego, CA)[55]. Side-chain replacement and modeling were carried out with the routine "Build mutant" of MODELLER 9v9.[56] $A\beta_{42}$ embodied a total of 15 point mutations whereas $A\beta_{40}$ contains 13 point mutations linked to familial Alzheimer's disease (FAD). A total of 10 conformations of each mutant were generated form four initial WT structures of $A\beta_{42}$ (1IYT and 1Z0Q) and $A\beta_{40}$ (1BA4 and 2LFM). In total, 560 mutant structures were created computationally for the 56 point mutations in $A\beta_{42}$ and $A\beta_{40}$.

Subsequently, these 560 structures were evaluated using DOPE (Discrete Optimized Protein Energy) scoring functions and PDF (Probability Density Function) total energy and finally 56 mutant structures were selected based on the lowest DOPE score and PDF total energy. DOPE score of a protein equates conformational energy which measures the relative stability of a conformation with respect to other conformations of the same protein. PDF Total Energy is the sum of the scoring function value of all homology-derived pseudo-energy terms and stereo chemical pseudo-energy terms. In total, 60 $A\beta_{42}$ and $A\beta_{40}$ structures (4 WT structures, 56 mutant structures) were subjected to further analysis.

Solvent Accessibility and Helical Percentage Calculation

Total solvent accessibility surface (Å^2) for all the 60 structures were calculated using DS 4.0 and other web-based tools; Get area[57], StrucTools (http://helixweb.nih.gov/structbio.html) and Mobyl[58, 59]. In addition to total solvent accessibility surface area, hydrophobic and hydrophilic solvent accessibility surface were also predicted using DS 4.0 for WT and mutant $A\beta_{42}$ and $A\beta_{40}$ structures. Furthermore, secondary structure analysis was carried for all the structures. Structural features such as helical geometry and percentage were calculated using PROMOTIF[60], available on the SWISS-MODEL web server.

Pre-processing of biochemical and clinical of data

Biochemical and patient data on disease onset (t_{onset}) and total steady-state Aβ levels measured during expression studies were collected from published data in original articles[61-75] and from the recently updated AD & FTD Mutation Database (http://www.molgen.ua.ac.be/ADMutations/).

Total Aβ steady-state levels were obtained by adding the reported $A\beta_{40}$ and $A\beta_{42}$ levels, which make up close to 100% of the isoforms. To put numbers from different experiments on the same scale, Aβ levels for WT were normalized to one. Experimental data for Aβ levels were extracted from Jonsson et al.[62] (A2T, A2V vs. WT), Chen et al.[66] (D7H), Nilsberth et al.[61] (E22G, E22K, E22Q, A21G), Zhou et al.[67] (E11K). Considering heterogeneous data for the A2V mutant, we also compared data from Jonsson et al.[62] which differs from Di Fede et al.[63], and data from Van Nostrand et al.[69] differ from data from Nilsberth et al.[61]

"Time of Onset" of WT and A2T Variant Carriers

Except WT and A2T disease onsets (t_{onset}), all other t_{onset} data are from the original sources. To enable an inclusion of the normal and protective phenotypes in the analysis, t_{onset} for WT carriers and A2T variant carriers were added as proxy numbers. According to United Nations Population Division 2010 report, the life expectancy of populations in developed regions is estimated to be 77.1 years. Appreciating the early-onset nature of the genetic risk factors, t_{onset} for WT should be higher than the average life span of the population from which (developed regions) clinical data on variants has been collected.

To test the sensitivity of the correlations to the choice of WT and A2T age of onset, this should reflect a normal healthy population average, a value of 75, 77 and 80 years for WT and also the A2T protective variant may increase longevity, and thus a value of 75, 77, 78, 80 and 83 years were considered. We tested the correlations of t_{onset} against 2LFM wild type and mutant hydrophobic surfaces using three different values for WT (75, 77 and 80 years) and five different values for A2T (75, 77, 78, 80 and 83 years).

These correlations are shown in Fig. S6 and it can be seen that these alternate numbers used to test the choice of WT and A2T age of onset have no significant effect on the overall correlation (Fig. S6). However, the United Nations Population Division has estimated that the life expectancy of populations in developed regions would increase to around 80 years towards 2015. Thus, t_{onset} = 75 for WT and t_{onset} = 80 for A2T were used throughout the paper. We conclude that reasonable choices of t_{onset} for WT and A2T consistent with their normal and protective phenotypes do not change the conclusions of our work, providing an external validation of the significance of our conclusions.

Statistical Treatment of Data

In the present study, correlation coefficients (R^2) and the *p*-values for linear correlations were used to identify statistically significant relationships. Statistical significance of all potential relations between clinical phenotypes (time of disease onset and total Aβ) and computed properties (total SAS, hydrophobic and hydrophilic surfaces) of WT and Aβ variants were examined. To this end, we have considered values of $R^2 > 0.3$ and $p < 0.05$ significant enough for discussion.

Acknowledgements

The authors acknowledge the Danish Technical University for providing a Hans Christian Ørsted (HCØ) fellowship to MKT.

Notes and references

Department of Chemistry, Technical University of Denmark, Kongens Lyngby 2800, Denmark.
Email: kpj@kemi.dtu.dk. Phone: (45) 45252419. Fax: 45883136

†Electronic Supplementary Information (ESI) available: [Figures S1−S4: wild type and mutant structural conformation for $A\beta_{42}$ and $A\beta_{40}$; Figure S6: effect of age of onset for wild type and A2T variant; Figures S7−S12: scatter graph plots for correlation between computed and experimental properties; Tables S1−S8: computed structural properties for wild type and mutant $A\beta_{42}$ and $A\beta_{40}$; Tables S9−S10: normalized data for t_{onset} and total Aβ where Aβ levels are from two sources; Tables S11−14: data for correlating t_{onset} with computed properties of wild type and mutant for $A\beta_{42}$ and $A\beta_{40}$; Table S15: total helix percentage calculated for WT and mutant $A\beta_{40}$ and $A\beta_{42}$; Tables S16−S19: data for correlating total Aβ with computed properties of wild type and mutant $A\beta_{42}$ and $A\beta_{40}$.]. See DOI: 10.1039/b000000x/

1 K. P. Kepp, *Chem. Rev.*, 2012, **112**, 5193-5239.
2 M. Eisenstein, *Nature*, 2011, **475**, S20-22.
3 G. M. McKhann, D. S. Knopman, H. Chertkow, B. T. Hyman, C. R. Jack, Jr., C. H. Kawas, W. E. Klunk, W. J. Koroshetz, J. J. Manly, R. Mayeux, R. C. Mohs, J. C. Morris, M. N. Rossor, P. Scheltens, M. C. Carrillo, B. Thies, S. Weintraub and C. H. Phelps, *Alzheimers Dement.*, 2011, **7**, 263-269.
4 S. Ayton, P. Lei and A. I. Bush, *Free Radic. Biol. Med.*, 2013, **62**, 76-89.
5 A. Rauk, *Chem. Soc. Rev.*, 2009, **38**, 2698-2715.
6 R. J. Guerreiro, D. R. Gustafson and J. Hardy, *Neurobiol. Aging*, 2012, **33**, 437-456.
7 D. E. Barnes and K. Yaffe, *Lancet Neurol.*, 2011, **10**, 819-828.
8 E. Levy-Lahad, W. Wasco, P. Poorkaj, D. M. Romano, J. Oshima, W. H. Pettingell, C. E. Yu, P. D. Jondro, S. D. Schmidt, K. Wang and et al., *Science*, 1995, **269**, 973-977.
9 L. Chávez-Gutiérrez, L. Bammens, I. Benilova, A. Vandersteen, M. Benurwar, M. Borgers, S. Lismont, L. Zhou, S. Van Cleynenbreugel, H. Esselmann, J. Wiltfang, L. Serneels, E. Karran, H. Gijsen, J. Schymkowitz, F. Rousseau, K. Broersen and B. De Strooper, *EMBO J.*, 2012, **31**, 2261-2274.
10 B. Schneider, D. Prvulovic, V. Oertel-Knochel, C. Knochel, B. Reinke, M. Grexa, B. Weber and H. Hampel, *Prog. Neurobiol.*, 2011, **95**, 703-717.

11 J. A. Hardy and G. A. Higgins, *Science*, 1992, **256**, 184-185.
12 G. M. Shankar and D. M. Walsh, *Mol. Neurodegener.*, 2009, **4**, 48.
13 E. Karran, M. Mercken and B. De Strooper, *Nat. Rev. Drug. Discov.*, 2011, **10**, 698-712.
14 R. Kayed, E. Head, J. L. Thompson, T. M. McIntire, S. C. Milton, C. W. Cotman and C. G. Glabe, *Science*, 2003, **300**, 486-489.
15 J. P. Cleary, D. M. Walsh, J. J. Hofmeister, G. M. Shankar, M. A. Kuskowski, D. J. Selkoe and K. H. Ashe, *Nat. Neurosci.*, 2005, **8**, 79-84.
16 S. Lesne, M. T. Koh, L. Kotilinek, R. Kayed, C. G. Glabe, A. Yang, M. Gallagher and K. H. Ashe, *Nature*, 2006, **440**, 352-357.
17 J. V. Rushworth and N. M. Hooper, *Int. J. Alzheimers Dis.*, 2011, **2011**.
18 S. Ohnishi and K. Takano, *Cell. Mol. Life Sci.*, 2004, **61**, 511-524.
19 E. Hubin, N. A. van Nuland, K. Broersen and K. Pauwels, *Cell. Mol. Life Sci.*, 2014, **71**, 3507-3521.
20 A. K. Paravastu, R. D. Leapman, W. M. Yau and R. Tycko, *Proc. Natl. Acad. Sci. U.S.A.*, 2008, **105**, 18349-18354.
21 M. Fandrich, M. Schmidt and N. Grigorieff, *Trends. Biochem. Sci.*, 2011, **36**, 338-345.
22 I. Bertini, L. Gonnelli, C. Luchinat, J. Mao and A. Nesi, *J. Am. Chem. Soc.*, 2011, **133**, 16013-16022.
23 H. A. Scheidt, I. Morgado, S. Rothemund, D. Huster and M. Fandrich, *Angew. Chem., Int. Ed. Engl.*, 2011, **50**, 2837-2840.
24 M. Ahmed, J. Davis, D. Aucoin, T. Sato, S. Ahuja, S. Aimoto, J. I. Elliott, W. E. Van Nostrand and S. O. Smith, *Nat. Struct. Mol. Biol.*, 2010, **17**, 561-567.
25 J. P. Colletier, A. Laganowsky, M. Landau, M. Zhao, A. B. Soriaga, L. Goldschmidt, D. Flot, D. Cascio, M. R. Sawaya and D. Eisenberg, *Proc. Natl. Acad. Sci. U.S.A.*, 2011, **108**, 16938-16943.
26 A. Jan, O. Adolfsson, I. Allaman, A. L. Buccarello, P. J. Magistretti, A. Pfeifer, A. Muhs and H. A. Lashuel, *J. Biol. Chem.*, 2011, **286**, 8585-8596.
27 E. Hellstrand, B. Boland, D. M. Walsh and S. Linse, *ACS Chem. Neurosci.*, 2010, **1**, 13-18.
28 Y. Miller, B. Ma and R. Nussinov, *Chem. Rev.*, 2010, **110**, 4820-4838.
29 S. Nag, B. Sarkar, A. Bandyopadhyay, B. Sahoo, V. K. Sreenivasan, M. Kombrabail, C. Muralidharan and S. Maiti, *J. Biol. Chem.*, 2011, **286**, 13827-13833.
30 D. J. Hayne, S. Lim and P. S. Donnelly, *Chem. Soc. Rev.*, 2014, **43**, 6701-6715.
31 A. Deshpande, E. Mina, C. Glabe and J. Busciglio, *J. Neurosci.*, 2006, **26**, 6011-6018.
32 R. M. Murphy, *Annu. Rev. Biomed. Eng.*, 2002, **4**, 155-174.
33 R. J. Morris, K. Eden, R. Yarwood, L. Jourdain, R. J. Allen and C. E. Macphee, *Nat. Commun.*, 2013, **4**, 1891.
34 M. Coles, W. Bicknell, A. A. Watson, D. P. Fairlie and D. J. Craik, *Biochemistry*, 1998, **37**, 11064-11077.
35 O. Crescenzi, S. Tomaselli, R. Guerrini, S. Salvadori, A. M. D'Ursi, P. A. Temussi and D. Picone, *Eur. J. Biochem.*, 2002, **269**, 5642-5648.
36 S. A. Kotler, P. Walsh, J. R. Brender and A. Ramamoorthy, *Chem. Soc. Rev.*, 2014.
37 R. Kayed and C. A. Lasagna-Reeves, *J. Alzheimers. Dis.*, 2013, **33**, S67-78.
38 L. M. Hou, H. Y. Shao, Y. B. Zhang, H. Li, N. K. Menon, E. B. Neuhaus, J. M. Brewer, I. J. L. Byeon, D. G. Ray, M. P. Vitek, T. Iwashita, R. A. Makula, A. B. Przybyla and M. G. Zagorski, *J. Am. Chem. Soc*, 2004, **126**, 1992-2005.
39 S. Mitternacht, I. Staneva, T. Hard and A. Irback, *Proteins*, 2010, **78**, 2600-2608.
40 A. Sandberg, L. M. Luheshi, S. Sollvander, T. Pereira de Barros, B. Macao, T. P. Knowles, H. Biverstal, C. Lendel, F. Ekholm-Petterson, A. Dubnovitsky, L. Lannfelt, C. M. Dobson and T. Hard, *Proc. Natl. Acad. Sci. U. S. A.*, 2010, **107**, 15595-15600.
41 D. Lambracht-Washington and R. N. Rosenberg, *Discov. Med.*, 2013, **15**, 319-326.
42 S. Vivekanandan, J. R. Brender, S. Y. Lee and A. Ramamoorthy, *Biochem. Biophys. Res. Commun.*, 2011, **411**, 312-316.
43 S. Tomaselli, V. Esposito, P. Vangone, N. A. van Nuland, A. M. Bonvin, R. Guerrini, T. Tancredi, P. A. Temussi and D. Picone, *ChemBioChem.*, 2006, **7**, 257-267.
44 M. K. Tiwari, R. K. Singh, R. Singh, M. Jeya, H. Zhao and J. K. Lee, *J. Biol. Chem.*, 2012, **287**, 19429-19439.
45 B. R. Brooks, C. L. Brooks, 3rd, A. D. Mackerell, Jr., L. Nilsson, R. J. Petrella, B. Roux, Y. Won, G. Archontis, C. Bartels, S. Boresch, A. Caflisch, L. Caves, Q. Cui, A. R. Dinner, M. Feig, S. Fischer, J. Gao, M. Hodoscek, W. Im, K. Kuczera, T. Lazaridis, J. Ma, V. Ovchinnikov, E. Paci, R. W. Pastor, C. B. Post, J. Z. Pu, M. Schaefer, B. Tidor, R. M. Venable, H. L. Woodcock, X. Wu, W. Yang, D. M. York and M. Karplus, *J. Comput. Chem.*, 2009, **30**, 1545-1614.
46 Y. Yoshiike, T. Akagi and A. Takashima, *Biochemistry*, 2007, **46**, 9805-9812.
47 B. Moores, E. Drolle, S. J. Attwood, J. Simons and Z. Leonenko, *PLoS One*, 2011, **6**, e25954.
48 J. Krishnamoorthy, J. R. Brender, S. Vivekanandan, N. Jahr and A. Ramamoorthy, *J. Phys. Chem. B.*, 2012, **116**, 13618-13623.
49 S. M. Butterfield and H. A. Lashuel, *Angew Chem. Int. Ed. Engl.*, 2010, **49**, 5628-5654.
50 S. A. Kotler, P. Walsh, J. R. Brender and A. Ramamoorthy, *Chem. Soc. Rev.*, 2014, **43**, 6692-6700.
51 M. F. M. Sciacca, S. A. Kotler, J. R. Brender, J. Chen, D. K. Lee and A. Ramamoorthy, *Biophys. J.*, 2012, **103**, 702-710.
52 A. Rijal Upadhaya, I. Kosterin, S. Kumar, C. A. von Arnim, H. Yamaguchi, M. Fandrich, J. Walter and D. R. Thal, *Brain*, 2014, **137**, 887-903.
53 A. Ramamoorthy and M. H. Lim, *Biophys. J.*, 2013, **105**, 287-288.
54 S. Lee, X. Y. Zheng, J. Krishnamoorthy, M. G. Savelieff, H. M. Park, J. R. Brender, J. H. Kim, J. S. Derrick, A. Kochi, H. J. Lee, C. Kim, A. Ramamoorthy, M. T. Bowers and M. H. Lim, *J. Am. Chem. Soc*, 2014, **136**, 299-310.
55 Accelrys Inc., 2013.
56 A. Sali and T. L. Blundell, *J. Mol. Biol.*, 1993, **234**, 779-815.
57 R. Fraczkiewicz and W. Braun, *J. Comp. Chem.*, 1998, **19**, 319-333.
58 C. Alland, F. Moreews, D. Boens, M. Carpentier, S. Chiusa, M. Lonquety, N. Renault, Y. Wong, H. Cantalloube, J. Chomilier, J. Hochez, J. Pothier, B. O. Villoutreix, J. F. Zagury and P. Tuffery, *Nucleic Acids Res.*, 2005, **33**, W44-49.
59 B. Neron, H. Menager, C. Maufrais, N. Joly, J. Maupetit, S. Letort, S. Carrere, P. Tuffery and C. Letondal, *Bioinformatics*, 2009, **25**, 3005-3011.
60 E. G. Hutchinson and J. M. Thornton, *Protein Sci.*, 1996, **5**, 212-220.

61 C. Nilsberth, A. Westlind-Danielsson, C. B. Eckman, M. M. Condron, K. Axelman, C. Forsell, C. Stenh, J. Luthman, D. B. Teplow, S. G. Younkin, J. Naslund and L. Lannfelt, *Nat. Neurosci.*, 2001, **4**, 887-893.

62 T. Jonsson, J. K. Atwal, S. Steinberg, J. Snaedal, P. V. Jonsson, S. Bjornsson, H. Stefansson, P. Sulem, D. Gudbjartsson, J. Maloney, K. Hoyte, A. Gustafson, Y. Liu, Y. Lu, T. Bhangale, R. R. Graham, J. Huttenlocher, G. Bjornsdottir, O. A. Andreassen, E. G. Jonsson, A. Palotie, T. W. Behrens, O. T. Magnusson, A. Kong, U. Thorsteinsdottir, R. J. Watts and K. Stefansson, *Nature*, 2012, **488**, 96-99.

63 G. Di Fede, M. Catania, M. Morbin, G. Rossi, S. Suardi, G. Mazzoleni, M. Merlin, A. R. Giovagnoli, S. Prioni, A. Erbetta, C. Falcone, M. Gobbi, L. Colombo, A. Bastone, M. Beeg, C. Manzoni, B. Francescucci, A. Spagnoli, L. Cantu, E. Del Favero, E. Levy, M. Salmona and F. Tagliavini, *Science*, 2009, **323**, 1473-1477.

64 K. Ono, M. M. Condron and D. B. Teplow, *J. Biol. Chem.*, 2010, **285**, 23186-23197.

65 Y. Hori, T. Hashimoto, Y. Wakutani, K. Urakami, K. Nakashima, M. M. Condron, S. Tsubuki, T. C. Saido, D. B. Teplow and T. Iwatsubo, *J. Biol. Chem.*, 2007, **282**, 4916-4923.

66 W. T. Chen, C. J. Hong, Y. T. Lin, W. H. Chang, H. T. Huang, J. Y. Liao, Y. J. Chang, Y. F. Hsieh, C. Y. Cheng, H. C. Liu, Y. R. Chen and I. H. Cheng, *PLoS One*, 2012, **7**, e35807.

67 L. Zhou, N. Brouwers, I. Benilova, A. Vandersteen, M. Mercken, K. Van Laere, P. Van Damme, D. Demedts, F. Van Leuven, K. Sleegers, K. Broersen, C. Van Broeckhoven, R. Vandenberghe and B. De Strooper, *EMBO Mol. Med.*, 2011, **3**, 291-302.

68 D. Kaden, A. Harmeier, C. Weise, L. M. Munter, V. Althoff, B. R. Rost, P. W. Hildebrand, D. Schmitz, M. Schaefer, R. Lurz, S. Skodda, R. Yamamoto, S. Arlt, U. Finckh and G. Multhaup, *EMBO Mol. Med.*, 2012, **4**, 647-659.

69 W. E. Van Nostrand, J. P. Melchor, H. S. Cho, S. M. Greenberg and G. W. Rebeck, *J. Biol. Chem.*, 2001, **276**, 32860-32866.

70 L. Miravalle, T. Tokuda, R. Chiarle, G. Giaccone, O. Bugiani, F. Tagliavini, B. Frangione and J. Ghiso, *J. Biol. Chem.*, 2000, **275**, 27110-27116.

71 T. Tomiyama, T. Nagata, H. Shimada, R. Teraoka, A. Fukushima, H. Kanemitsu, H. Takuma, R. Kuwano, M. Imagawa, S. Ataka, Y. Wada, E. Yoshioka, T. Nishizaki, Y. Watanabe and H. Mori, *Ann. Neurol.*, 2008, **63**, 377-387.

72 L. Obici, A. Demarchi, G. de Rosa, V. Bellotti, S. Marciano, S. Donadei, E. Arbustini, G. Palladini, M. Diegoli, E. Genovese, G. Ferrari, S. Coverlizza and G. Merlini, *Ann. Neurol.*, 2005, **58**, 639-644.

73 D. A. Carter, E. Desmarais, M. Bellis, D. Campion, F. Clerget-Darpoux, A. Brice, Y. Agid, A. Jaillard-Serradt and J. Mallet, *Nat. Genet.*, 1992, **2**, 255-256.

74 C. T. Jones, S. Morris, C. M. Yates, A. Moffoot, C. Sharpe, D. J. Brock and D. St Clair, *Nat. Genet.*, 1992, **1**, 306-309.

75 Y. Tomidokoro, A. Rostagno, T. A. Neubert, Y. Lu, G. W. Rebeck, B. Frangione, S. M. Greenberg and J. Ghiso, *Am. J. Pathol.*, 2010, **176**, 1841-1854.

Graphical abstract

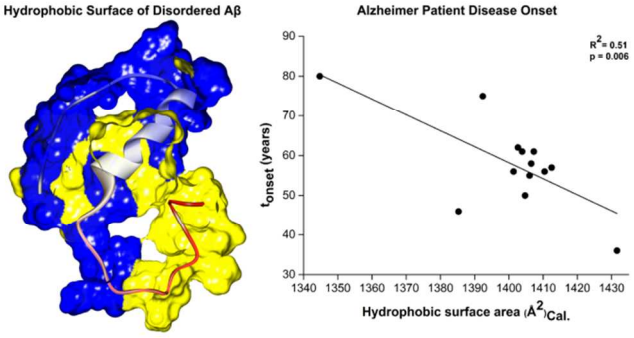

Direct correlation of Alzheimer patient data to a spectrum of NMR structures and chemical properties of beta amyloid (Aβ) variants allows identification of conformation-dependent disease properties.